Development of corrosion-free concrete beam-column joint with adequate seismic energy dissipation

M. Nehdi[1], M. Shahria Alam[2], and M.A. Youssef[3]

[1, 3]Department of Civil and Environmental Engineering, The University of Western Ontario
London, Ontario, Canada N6A 5B9

[2]School of Engineering-Okanagan, The University of British Columbia
Kelowna, BC, Canada V1V 1V7

Abstract

The use of Fibre−Reinforced Polymer (FRP) as reinforcement in concrete structures has received much attention owing to its higher resistance to corrosion compared to that of regular steel reinforcement. Since FRP is a brittle material, its use in seismic resisting structural elements has been a concern. FRP RC structures can be made ductile by utilizing a ductile material such as steel at the plastic hinge regions. However, the use of steel negates the corrosion resistance purpose of FRP. On the other hand, Nickel-Titanium (Ni-Ti) shape memory alloy (SMA) is highly resistant to corrosion. It also brings about an added advantage in seismic regions since it has the unique ability to undergo large deformation, but can regain its un-deformed shape through stress removal. In this study, a SMA-FRP hybrid RC beam-column joint has been proposed to address not only corrosion resistance, but also seismic related problems. This joint is reinforced with super-elastic Ni-Ti SMA bar at the plastic hinge regions of the beam and FRP in the other regions of the beam and column. To validate the proposed joint, an experimental investigation has been carried out to develop such a joint and test it under reversed cyclic loading. The results are compared in terms of load-storey drift, moment-rotation and energy dissipation capacity to those of a similar RC beam-column joint specimen reinforced with conventional steel. The SMA-FRP beam-column joint proved to have adequate energy dissipation under earthquake type loading.

Keywords: FRP, SMA, super-elasticity, beam-column joint, corrosion, ductility, seismic.

[1] Corresponding author. Email: mnehdi@eng.uwo.ca, Fax: 519-661-3779, Phone: 519-661-2111 Ext.: 88308.

1. INTRODUCTION

Steel has been used as reinforcement in concrete structures for more than a century. However, corrosion of steel is a major problem and has been responsible for the early deterioration of reinforced concrete (RC) structures. Recently, a number of bridge structures in North America collapsed in which corrosion of steel has been identified as the root cause of failure. Billions of dollars are spent annually for the rehabilitation of civil infrastructure, especially in the replacement of corroded steel. In order to mitigate such a problem, fiber-reinforced polymer (FRP) bars have been introduced as reinforcement for concrete, and this has been an important research subject matter over the last two decades. Since FRP is a brittle material, it fails within its elastic range with no inelastic branch. Thus, FRP RC structures exhibit a predominantly elastic behavior with low energy dissipation capacity, which is considered as a major problem in seismic design (Said and Nehdi 2004). Moreover, FRP bars typically exhibit weaker bond to concrete compared to that of similar steel bars. The bond between FRP and concrete can be ameliorated with the help of mechanical anchorages, e.g. sand coating or surface deformations. However, the use of FRP in RC structures is still a concern, in seismic regions where the energy dissipation capacity of a structure is one of the most important design issues. Although steel (within its elastic range) and FRP RC elements are expected to behave in a comparable fashion since their behaviour basically depends on the bond between reinforcing bars and concrete, the low modulus of elasticity of FRP is responsible for causing larger deflections of RC members compared to that of similar steel RC elements. The absence of yielding and an inelastic branch in the stress-strain behaviour of FRP can result in a sudden and brittle failure without adequate warning and with little dissipation of energy. Thus, it is

questionable to use FRP RC elements in seismic regions without additional means of energy dissipation.

If FRP RC structures can dissipate significant amounts of energy during seismic loading and have adequate ductility, their use will not only mitigate the problem of corrosion, but can also make the structure safe as it will provide adequate warning before failure, thus, enhancing the confidence level of designers in such applications. An experimental investigation was carried out where a RC beam-column joint reinforced with SMA at the plastic hinge region of the beam and steel in the other regions was constructed and tested. The results showed that the joint could dissipate a significant amount of energy, yet suffered only negligible residual drift, and minor repairing work could regain its full load carrying capacity (Youssef et al. 2008).

In the present study, the authors propose to achieve ductility in FRP RC structural member by using a ductile material such as steel, stainless-steel or a shape memory alloy placed at the plastic hinge regions of the member, whereas FRP bars can be used in the other regions. Due to its low corrosion resistance, regular steel may not be an optimal solution; while stainless steel can be taken into consideration. Shape memory alloy (SMA) is a material that is highly resistant to corrosion. Moreover, super-elastic (SE) SMA is a unique alloy with the ability to undergo large deformation, but can regain its un-deformed shape through stress removal. Using stainless steel along with FRP bars can reduce maintenance and repair costs since there will be no significant corrosion. However, if the structure is subjected to a strong earthquake, stainless steel will undergo inelastic deformation and will not be able to recover its original shape, thus, experiencing permanent deformation. On the other hand, the use of SMA as

reinforcement will not only eliminate the corrosion problem, but can also allow recovering inelastic deformation at the end of earthquakes. Hence, SMA/FRP RC structural elements can possibly sustain repeated earthquake loading even though the SMA bar is being strained beyond its yield limit. In contrast, stainless steel will accumulate deformation and the structure can lose its serviceability. Nevertheless, stainless steel is currently less costly compared to SMA.

Little or no research has been directed towards splicing of FRP bars with another ductile material and using such spliced connections in a beam-column joint (BCJ) so as to make the structure ductile with enhanced deformation capacity. In this study, a suitable coupler has been developed for splicing FRP with SMA bar, then the FRP spliced SMA bar was used as reinforcement in a beam column joint. The prime objective of this study is to investigate the seismic behaviour of a concrete BCJ reinforced with SE SMA in its plastic hinge zone and FRP in its other regions, and compare its performance to that of a regular steel RC BCJ in terms of load-displacement, moment-rotaton and energy dissipation capacity, and strains in the longitudinal and transverse reinforcements.

2. RESEARCH SIGNIFICANCE

There has been a growing interest in the use of FRP bar as reinforcement for concrete structures because of its higher resistance to corrosion compared to that of steel. Although steel-free FRP RC can mitigate the problem of reinforcement corrosion, it may not provide adequate safety in seismic regions due to its reduced ductility. Hence, FRP RC structures need to be designed in such a way that they possess higher reserve of strength [ACI 440.1R-06

2006]. Two seismic design approaches may be considered. Either the safety margin can be increased ensuring elastic behaviour under service load, or the safety margin can be reduced while maintaining elastic behaviour under service loads by over-reinforcing members with FRP bars in order to prevent bar rupturing [Sharbatdar and Saatcioglu 2009]. In both cases, the sections will be overdesigned to withstand such seismic forces, which will result in excessive cost substantial wastage of material. Hence, ductility is a major concern for the seismic design of the relatively less ductile FRP RC structures. Indeed, there is an important need to induce ductility in FRP RC members, which will not only make such structures highly resistant to corrosion, but also capable of dissipating significant amounts of energy during earthquakes. Hybrid RC structures in which FRP reinforcement is spliced with a ductile material can be a potential solution to this problem. Yet, this requires rigorous experimental investigations on such hybrid FRP RC structures to understand its inelastic behavior, ductility and energy dissipation capacity under seismic loading. Thus, the present study should assist structural engineers in designing hybrid FRP RC members, with a potential to mitigate several problems associated with infrastructure management against both corrosive environments and seismic loading.

3. SCOPE OF PREVIOUS WORK

The use of FRP as reinforcement in RC elements was investigated by various researchers for instance in RC frames [Fukuyama et al. 1995], columns [Grira and Saatcioglu 1999; Choo 2005; Cole and Fam 2006], ground anchorage [Benmokrane et al. 2000], beams [Toutanji and Saafi 2000; Salib and Abdel-Sayed 2004], beam-column joints [Nehdi and Said 2005], bridge decks [Berg 2006], and slabs [Udhayakumar et al. 2007]. Due to the limited ductility of FRP

RC elements, various researchers have investigated the use of hybrid steel-FRP reinforcements. Aiello and Ombres [2002] tested six beams with different configurations of longitudinal bar of steel only, FRP only, and hybrid FRP-steel. Steel stirrups were used in all specimens. Experimental results showed that the hybrid reinforced beams experienced higher ductility but lower service deflection than that of the steel-free FRP beam. Leung and Balendran [2003] tested seven steel and GFRP RC beams under four point bending with varying concrete strength and reinforcement ratios so as to produce under-reinforced and over-reinforced sections. The study showed that in the case of hybrid beams, steel contributed more efficiently to the overall performance up to yielding, then the stiffness of steel dropped significantly and the GFRP bars started to contribute more effectively to the section resistance. In the case of beams made of higher strength concrete, the improved flexural capacity resulted in shifting the flexural failure to a shear failure. Nehdi and Said [2005] used glass FRP as reinforcement in beam-column joints. They tested a steel free GFRP and a hybrid GFRP-steel RC beam-column joints under reversed cyclic loading. The beam cross-section of the hybrid specimen had three GFRP bars and three steel bars as its top and bottom longitudinal reinforcements, respectively. The test results showed that the failure of FRP RC BCJ took place in a sudden and brittle manner when two of the beam's bottom GFRP bars snapped in tension. In the case of the hybrid BCJ specimen, one out of three GFRP bars failed in tension, whereas the other two slipped out of the joint. The hybrid specimen exhibited higher stiffness and energy dissipation capacity compared to that of the steel-free GFRP RC BCJ.

Saikia et. al [2005] introduced hybrid bars consisting of glass fiber-reinforced polymer (GFRP) strands of 2 mm diameter wound helically on a mild steel core of 6 mm diameter as reinforcement in normal-strength concrete beams. It was observed from the test that the hybrid RC beam exhibited lower stiffness compared to that of steel RC beam. Failure of hybrid RC beams was primarily due to delamination of concrete at the reinforcement level, leading to anchorage failure, resulting in loss of bond between the hybrid bar and concrete. Won and Park [2006] introduced a special type of hybrid braided FRP bar, which consisted of a core FRP bar with braiding yarn wound around it, and this bar appears to be a promising solution to the brittle failure of FRP. However, more research is required on hybrid braided FRP reinforced concrete structures before introducing this practice in full-scale construction.

Substantial research has been done over the last two decades on the possible uses of SMAs in structural applications [Alam et al. 2007a, 2008]. Since SMA is a costly material compared to reinforcing steel, it was not until 2004 that it found its way as reinforcement in concrete [Wang 2004]. Saiidi and Wang [2006] used SMA rods in the plastic hinge area of RC columns and evaluated the seismic performance of these columns. Two ¼-scale spiral RC columns with SMA longitudinal reinforcement in the plastic hinge area were designed for laboratory shake table testing. When used as reinforcement in critical RC structural elements, SMAs can yield under strains caused by seismic loads, but potentially recover deformations at the end of earthquake events [Saiidi and Wang 2006; Alam et al. 2007b; Youssef et al. 2008;], thus, requiring a minimum amount of repair work [Saiidi and Wang 2006]. The properties of SMAs including their high strength, large energy hysteretic behaviour, full

recovery of strains up to 8%, and high resistance to corrosion and fatigue make them strong contenders for use in earthquake resistant structures [Wilson and Wesolowsky 2005]. In particular, Ni-Ti alloy has been found to be the most promising SMA for seismic applications [Alam et al. 2007c].

4. EXPERIMENTAL PROGRAM

Two ¾-scale BCJ specimens are considered in this study. One is reinforced with regular steel bars (specimen JBC-1), while the other is reinforced with SMA at the plastic hinge region of the beam along with GFRP bar in the remaining portion of the joint (specimen JBC-4). Both joints were constructed and tested at the Structures Laboratory of the University of Western Ontario.

4.1 Specimen Details

An eight-storey RC building with moment resisting frames was designed and detailed in accordance with Canadian Standards [CSA A23.3-04 2004]. The building was assumed to be located in the western part of Canada on firm ground with un-drained shear strength of at least 100 kPa. The elevation and plan of the building are shown in Fig. 1. The moment frames were designed with a moderate level of ductility. An exterior beam-column joint was isolated at the points of contra-flexural, from the mid-column height of the fifth floor to the mid-column height of the sixth floor (Joint A in Fig. 1).

The size of the BCJ test specimens was reduced by a factor of ¾ to account for limitations of laboratory space and testing equipments. The forces acting on the joints were also scaled

down by a factor of $(¾)^2$. This factor was chosen to maintain normal stresses in the scaled models similar to that of the full-scale joint. The beam and column were designed with the maximum moment and shear forces developed considering all code specified load combinations. The design column axial force, *P,* was 620 kN and the scaled down *P* became 350 kN. The detailed design of the joints is given in Fig. 2.

The geometry, longitudinal and transverse reinforcement arrangements were similar for both specimens. The reduced cross-section of the column was 250 mm by 400 mm with longitudinal 4-M20 (diameter: 19.5 mm) steel rebars in JBC-1 and 4-#6 (diameter: 19.1 mm) FRP rebars in JBC-4, corresponding to 1.19% and 1.15% reinforcement ratio, respectively. The columns were transversely reinforced with M10 (diameter: 11.3 mm) closed steel stirrups for JBC-1 and #3 (diameter: 9.5 mm) closed GFRP rectangular ties for JBC-4, spaced at 80 mm in the joint region and for a distance of ±640 mm from the face of the joint, in both cases. The spacing of the ties for the remaining length of the columns was 115 mm.

SE SMA was used as longitudinal reinforcement at the plastic hinge region of the beam in JBC-4. The top and bottom longitudinal reinforcements were 2-SMA20 (diameter: 20.6 mm) bars (reinforcement ratio = 1.33%). The size of SMA bar was chosen such that the SMA section had slightly lower moment carrying capacity compared to that of the FRP section and yielding does initiate in the SMA bar before rupture of the FRP bar. The plastic hinge length was calculated [Paulay and Priestley 1992] as 360 mm from the face of the column, which includes an additional length of 50 mm to hold the bar inside the coupler in the joint (Fig. 3). Mechanical couplers were used to connect SMA bars and FRP bars (Fig. 3). The total length

of SMA bars was 450 mm from the centre to the coupler in the joint to the coupler in the beam as shown in Fig. 3. The ties of the beams were spaced at 80 mm for 800 mm length adjacent to the column and then spaced at 120 mm. The size of the longitudinal bar and the size and spacing of the transverse reinforcement for the joint conformed to current code requirements [CSA A23.3-04 2004].

4.2 Materials

Concrete: Both specimens were cast with highly flowable ready-mix concrete with a slump of 720 mm and 735 mm (inverted cone method) for JBC1 and JBC4, respectively. The air content of fresh concrete was 5.5%. The concrete compressive strength at the time of testing was 53.5 MPa and 45.7 MPa for specimens JBC1 and JBC4, respectively. The split cylinder tensile strength for JBC-1 and JBC-4 was 3.5 and 3.0 MPa, respectively.

Steel Bar: Tensile strength tests of steel bars of JBC1 were also performed in the laboratory. The yield strength, ultimate strength, and Young's modulus were 520 MPa, 630 MPa, and 198 GPa, respectively for 20M steel reinforcing bars. The steel bars used for ties were 10M with a yield strength and ultimate strength of 422 MPa and 682 MPa, respectively.

FRP Bar: In this study, glass fiber-reinforced polymer (GFRP) bar (also known as V-Rod) was used. The surface of the bar was sand coated so as to improve the bond between concrete and FRP. The binding material of the GFRP bar is composed of modified vinyl ester resin with a maximum volume fraction of 35%, along with continuous e-glass fibers with a minimum volume fraction of 65%. The manufacturer's specified design tensile strength,

ultimate strength and tensile modulus are 656 MPa, 728 MPa and 47.6 GPa, respectively. The GFRP's coefficient of thermal expansion was specified as $6x10^{-6}/^{o}C$. Cyclic tensile tests were performed on the spliced GFRP bar with epoxy adhesive in the universal testing machine. It was not possible to conduct the test up to the rupture of the GFRP bar as the connection failed due to sliding of the GFRP bar from the coupler. The test result (Fig. 4a) shows that the connection failed by sliding out of the GFRP bar at a stress of 577 MPa. The tensile modulus of the GFRP bar was 52.2 GPa, which was higher than the specified value.

SMA Bar: Hot-rolled Ni-Ti alloy bar was used as reinforcement in the JBC-4 specimen. It has an average of 55.0% nickel and 45.0% titanium by mass. Its austenite finish temperature, A_f, defining the complete transformation from martensite to austenite, ranges from -15°C to -10 °C. Above this temperature, the alloy is within the super-elastic range. Each Ni-Ti bar used in this study was 450 mm long and 20.6 mm in diameter. Figure 4b shows the stress-strain behaviour of the SMA while testing the SMA splice connection. This figure shows the cyclic tensile behaviour of the SMA up to its super-elastic strain of 5%, where the characteristic stress-strain curve shows a flag-shaped response. Although SMA does not have a yielding process, yield is being used in this study to refer to the initiation of phase transformation of SMA. The yield point is identified as 401 MPa (f_{y_SMA}), which reached at 0.64% strain (ε_y) at a slope of 62.5 GPa (Young's modulus, E). This yield strength has been defined from an idealized bilinear elastic-plastic SMA stress-strain model with kinematic strain hardening. In actual stress-strain curve f_{y_SMA} reached at a strain of 1.35%. Since the splice connection failed due to failure of the FRP connection, the bar was tested only up to 5% strain, and a residual strain of 0.58% was observed. Since the modulus of elasticity of SMA and FRP are about

one-third that of steel, the SMA-FRP RC specimen is expected to experience higher strains than that of the steel specimen at a similar load level.

4.3 Splicing Technique of FRP with SMA bar

The splicing of FRP bar with a ductile material like SMA bar was one of the major challenges for this experimental program. There was no readily available mechanical coupler that can connect brittle FRP bar with another ductile material. A regular screw-lock coupler (Fig. 5) was tested for splicing and it was found that the sharp end of the screw ruptures the top fibres of the GFRP bar. Flattened screws were also used but did not work as the FRP bar was not strong enough to take normal forces in the perpendicular direction of the orientation of fibres and the fibres were easily damaged. Therefore, a viable option was to use an adhesive type coupler for the sand coated FRP bar.

An adhesive type coupler was also tested for connecting SMA bars to FRP bars. Since this type of coupler resists forces solely by friction, the SMA bar slipped out easily while being pulled because of its smooth surface. Therefore, mechanical anchorages were considered for connecting SMA to the steel coupler. Machining large diameter bars of Ni-Ti using conventional equipment and techniques is extremely difficult due to its high hardness. Although there are various ways of welding and soldering Ni-Ti, e.g. using e-beam, laser, resistance and friction welding, and brazing with Ag-based filler metals; welding Ni-Ti to steel couplers is much more problematic because of the development of a brittle connection around the weld zone [Hall 2003]. Weld deposits with Ni-filler metal have exhibited sufficient tensile strength allowing SE deformation of Nitinol [Hall 2003]. Threading large

diameter nitinol bars reduces its strength due to its sensitivity to notches. Therefore, instead of threaded couplers, bar lock couplers with flat shear bolts have been used. Several couplers having variable number of screws and different arrangements were tested. It was found that nine-5 mm diameter flat end screws arranged in three rows were adequate to minimize the relative slippage between the bar and the coupler. Finally, the coupler that was used in the specimen JBC-4 had two parts: one was a stainless steel pipe filled with epoxy resin for holding the FRP bar and the other one was a screw-lock coupler for holding the SMA bar as shown in Fig. 6 (a). This new hybrid coupler is named "screw lock-adhesive type coupler". Figure 6 (b) shows the test setup of the spliced connection for FRP-SMA bar. A simple pullout test was performed to determine the slippage of SMA and FRP bars inside the coupler. The stress versus slippage of SMA and FRP bars is shown in Fig. 7 (a) and (b), respectively. In each case the result shows that the slippage inside the coupler was not significant at the initial stage of loading. The slippage increased with the increase of the load, and the coupler failed by sliding out of the FRP bar from the coupler. However, the connection was found suitable to carry the required load for the test as predicted from the numerical analysis. After successful testing of the spliced connection, the reinforcement cage was prepared where the splice details in JBC-4 and the rebar cage inside the formwork are shown in Figs. 8 and 9, respectively.

4.4 Loading

A constant axial load was applied at the top of the column and a reversed quasi-static cyclic load was applied at the beam tip. The load history applied at the beam tip consisted of a load-controlled phase followed by a displacement-controlled loading phase. During the load-

controlled phase, two load cycles were applied at 10% of the theoretical yield load of the beam to ensure that the data acquisition system is functioning properly. The following load control cycles (4 cycles) were applied to define the loads causing flexural cracking in the beam (2 cycles) and yielding of its longitudinal bars (2 cycles). The yield load, P_y, and the yield displacement, Δ_y, were recorded. After yielding, displacement-controlled loading was applied. For each load cycle, the test specimen was subjected to two identical complete cycles to ensure stability. Tests were conducted up to a storey drift of at least 4%, which is more than the collapse limit defined by Elnashai and Broderick [1994].

4.5 Test setup and Instrumentation

Figure 10 illustrates a schematic diagram of the specimen, the test rig, and the reaction frame. The bottom of the column was hinged with pins penetrating through a sleeve with narrow holes. A roller support was created at the top of the column with pins penetrating through a sleeve with 20 mm vertical slots. The load cycles were applied at the beam tip using an actuator, which was pin connected at the beam-tip. The arm length was measured as 1870 mm from the pin connection to the mid column line. Figure 10 also illustrates the instrumentation of test specimens. Two load cells were used to measure the column axial load and beam tip load. During testing, displacements were measured at various locations using linear variable displacement transducers (LVDTs). One pair of LVDT was attached to the joint area to measure the joint distortion. The other two LVDTs were placed in parallel on the top and bottom of the beam at a distance of 180 mm away from the column face to measure beam rotation. The displacement was measured at the free end of the beam using a string potentiometer. For both specimens, electrical resistance strain gauges were installed on the

main reinforcing bars and transverse reinforcement of the beam and column as shown in Fig. 2. A portable computer attached to the data acquisition system was used to record readings at a constant time interval with one reading per second.

5. Experimental Results

5.1 Specimen JBC-1

Figure 11 shows the beam tip load versus storey drift relationship of specimen JBC-1. The First Flexural Crack (FFC) was observed at the top of the beam near the column face at a beam tip-load of 11.7 kN, corresponding to a drift of 0.22%. The first diagonal crack in the joint appeared close to the first flexural crack at a beam tip load of 30.0 kN, corresponding to a drift of 0.66 %. Additional cracks occurred at the joint with the progress of loading. However, all the cracks in the joint region were of very fine width streaming from the first two cracks that emerged along the diagonals. The top longitudinal bar of the beam first yielded at a beam tip-load of 51.3 kN with a corresponding yield displacement, Δ_y of 12 mm (drift of 1.3%). At 2.6% storey-drift, the beam suffered a relatively wide flexural crack at the column face that extended its full depth along with some minor cracks that formed parallel to the column face. At a storey-drift of 4%, the crack at the column face widened and two relatively large cracks almost parallel to the column face became more evident at distances of approximately 180 mm and 300 mm from the column face, respectively. Figure 12 shows the crack pattern of JBC-1. Throughout the test, the axial load of the column was maintained and the joint area remained fully undamaged apart from few hairline cracks (Fig. 12).

5.2 Performance of JBC-4

Figure 13 shows the load-storey drift relationship of the FRP-SMA RC beam-column joint specimen JBC-4. The FFC was detected at the bottom of the beam at 72 mm away from the column face at a drift of 0.22%. In the subsequent cycle having the same drift; another crack developed at the top of the beam at a distance of 85 mm away from the column face and extended meeting the first crack. Thus, a single fine crack was formed and extended over the full beam-depth. With the progress of loading, several flexural cracks occurred at the top and bottom of the beam along a length of 900 mm measured from the column face. At a drift of 0.66%, the FFC opened up to a width of 0.5 mm at the bottom of the beam, but it could fully close after unloading. A fine crack took place in the joint region at a beam tip-load of 26 kN corresponding to a drift of 0.99%. While subjected to a drift of 1.32%, the FFC opened up to 1.2 mm, and the residual crack width was zero after unloading. It was observed that the bottom SMA bar reached its yield strain (1.35%) at a beam tip-load of 34.1 kN and a drift of 1.97%. In this case, the corresponding yield displacement, Δ_y was 18 mm. At this stage the opening sizes of the FFC were 1.5 mm and 1.0 mm, where the residual crack widths were 0.1 mm and 0.05 mm at the bottom and top of the BCJ specimen, respectively. At a drift of 2.73%, a crack formed at the face of the column and propagated deeper into the beam. Some minor cracks also streamed out of the FFC toward the column face. The FFC also started to grow wider and reached a width of 3.6 mm at the outer face at a drift of 3.28%. When the displacement cycle reached a zero value, the FFC width became smaller and it was generally less than 0.85 mm. At a drift of 4.4%, the FFC opened up to 5.4 mm and later closed to a width of less than 1.5 mm. The joint region exhibited a few cracks of fine width and small length, and remained nearly intact. Figure 14 shows the crack pattern of JBC-4.

6. PERFORMANCE COMPARISON BETWEEN JBC-1 AND JBC-4

This section compares the performance of JBC-1 and JBC-4 in terms of load-displacement, moment-rotation, energy dissipation capacity (Table 1) and measured strains in bars.

6.1 Load-storey drift envelope

The beam-tip load versus storey drift envelope of both specimens JBC-1 and JBC-4 exhibited typical elasto-plastic behavior as depicted in Fig. 15. Although they started with comparable stiffness, the FRP-SMA RC specimen experienced a drop in its stiffness after the occurrence of the first flexural crack. This is due to SMA's lower Young's modulus compared to that of steel. However, both specimens showed comparable load carrying capacity at a drift of about 3.0%. Beyond a drift of 3%, there was a slight decrease in the tip load in the case of JBC-4, which might be due to the slippage of SMA bars inside the couplers at the joint region. At 4% drift, JBC-4 had 15% lower load capacity compared to that of JBC-1. It is to be noted that even beyond 4% drift, JBC-4 could carry more than 50 kN of tip load. Comparing Figs. 11 and 13, it can be observed that JBC-1 experienced lower residual drift (1.8%) compared to that of JBC-4 (2%). This might be because of slippage of FRP bars inside the couplers. However, the beam tip of JBC-4 after final unloading could regain its original position as its rebar at the plastic hinge region experienced negligible residual strain and was serviceable and repairable whereas JBC-1 experienced significant permanent deformation in its beam tip and plastic set in its rebar at the plastic hinge region and was not serviceable or repairable.

6.2 Cumulative energy dissipation

The cumulative energy dissipated by the specimens during reversed cyclic loading was calculated by summing up the dissipated energy in successive load-displacement loops throughout the test. The cumulative energy dissipation with respect to storey drift for specimens JBC-1 and JBC-4 is depicted in Fig. 16. JBC-1 dissipated 3.4 kN.m of energy at a storey drift of 3% (collapse limit as defined by Elnashai and Broderick 1994), whereas JBC-4 dissipated 3.1 kN.m of energy. At a storey drift of 4%, JBC-4 dissipated 6.29 kN.m of energy, while JBC-1 dissipated 6.76 kN.m of energy, which is only 7.5% higher compared to that of JBC-4. The amount of energy dissipated at 4% storey drift for JBC-1 is equivalent to the amount of energy dissipated by JBC-4 at a storey drift of 4.1%. The results show that JBC-4 could dissipate a comparable amount of energy compared to that of JBC-1 at different storey drifts. The level of damage in JBC-4 indicates that the FRP-SMA RC joint suffered extensive cracking in the beam hinge region (Fig. 14) and there were significant slippage of bars inside the concrete, which helped dissipating a comparable amount of energy to that of JBC-1. The steel RC joint dissipated energy through larger hysteretic loops of steel bar compared to that of SE SMA bar, whereas in the case of the FRP-SMA RC joint, slippage of SMA and FRP bars from couplers and larger width cracks in beams helped to dissipate a comparable amount of energy to that of the steel RC joint (Figs. 11-14).

6.3 Beam rotations

Two LVDTs were mounted on the top and bottom of the beam at a distance of 180 mm from the column face (Fig. 10) in order to measure beam rotations at the plastic hinge region. The beam rotations with respect to the applied moment for JBC-1 and JBC-4 are presented in Figs. 17a and 17b, respectively. Figure 18 shows the positive moment and beam rotation envelopes

of both specimens. The results illustrate that specimen JBC-4 experienced significant rotation before yielding of SMA compared to that of JBC-1. This increase in rotation is mainly due to the lower stiffness of SMA bar compared to that of steel. At a storey-drift of 4%, JBC-4 suffered larger beam rotation of 0.0095 rad compared to 0.006 rad for JBC-1. JBC-4 also suffered higher residual beam-rotation (0.012 rad) compared to that of JBC-1 (0.0042 rad).

6.4 Measured strains in bars

Strains were measured in both longitudinal and transverse reinforcing bars. Figures 19a and 19b show the measured strains in the main top reinforcing steel and SMA bar at the plastic hinge region, close to the column face of specimens JBC-1 and JBC-4, respectively. Figure 19a shows that specimen JBC-1 suffered high residual strain (6450 μ-strain) in the top bar beyond its yield load, whereas Fig. 19b illustrates that JBC-4 experienced a much smaller residual strain (1510 μ-strain) despite that it was subjected to larger strain. For specimen JBC-4, SMA bars were placed close to the face of the column and its low modulus of elasticity compared to that of steel resulted in higher strain in the plastic hinge region, causing a major crack away from the column face. For specimen JBC-1 the maximum measured strain in the main steel reinforcing bar inside the joint was 1906 μ -strain with wider loops of strain, whereas the FRP bar inside the joint of specimen JBC-4 experienced 3861 μ-strain with narrower loops. Although FRP bar was supposed to experience at least three times strain compared to that of steel bar, its lower strain might be due to transferring a portion of the force in the SMA bar to the concrete through bearing of the coupler.

The maximum measured strain in the transverse reinforcement inside the joint of JBC-1 was 684 μ-strain, while the corresponding maximum value for specimen JBC-4 was about 890 μ-strain. This difference in the strain distributions is likely due to the slippage of FRP and SMA bars in couplers that changed the distribution of shear strains within the joint. It is evident that SMA bar in JBC-4 suffered much lower residual strain compared to that of steel in JBC-1. However, this contradicts the load-storey drift relationships since the results show that JBC-4 suffered higher residual deformation, i.e. both displacement and rotation (Figs. 13 and 17 b) compared to that of JBC-1 (Figs. 11 and 17 a), which might be due to significant slippage of FRP bars inside the couplers.

7. COMPARISON OF PERFORMANCE OF STEEL TO FRP ONLY, AND TO FRP-SMA RC BCJS

Said and Nehdi [2004] tested a steel RC BCJ (J1) and a FRP RC BCJ (J4) under reversed cyclic loading, which had similar dimensions and reinforcement ratio. Figure 20 shows the load-storey drift envelopes of J1 and J4 up to 4% drift where after cracking the FRP RC BCJ exhibited lower stiffness and strength compared to that of the steel RC BCJ. J4 essentially showed an elastic envelope compared to that of the elastic-plastic curve of J1, which indicates that FRP RC BCJs will not provide adequate warning before failure because of its limited ductility, whereas the FRP-SMA RC BCJ exhibited a gradual descending branch after reaching its peak load and thus, could provide adequate ductility before failure (Fig. 15). Figure 21 shows the cumulative energy dissipation capacities of J1 and J4 up to 4% drift. The results show that at 4% drift, the FRP RC BCJ dissipated 74% less energy compared to that of

the steel RC BCJ because of the lower hysteretic loop of the FRP RC specimen, whereas the FRP-SMA RC BCJ could dissipate almost an equal amount of energy to that of the steel RC BCJ (Fig. 16). Thus, FRP-SMA RC BCJs would perform better than FRP RC BCJs in terms of ductility and energy dissipation capacity.

8. DISCUSSION

The use of coupled FRP-steel or FRP-SMA as reinforcement in concrete is yet to be introduced in real structural applications. Before the full-scale use of such coupled reinforcements in the industry, significant experimental efforts are still required for establishing proper guidelines to connect different types of bars of various diameters. In the case of the chemical/adhesive type coupling mechanism, the length of the splice is an important factor that needs to be determined from further testing. Alternative mechanical coupling mechanisms for FRP bar needs to be developed, which could provide better results in terms of reducing slippage compared to that of chemical/adhesive type coupler.

The relatively high cost of SMA is a restraining factor that hinders its wide spread use in the construction industry. However, there has been a significant reduction in the prices of Ni-Ti over the last ten years, from more than 1000 USD to below 150 USD per kg at present. The price is still considerably higher than that of other construction materials. However, SMA can be used along with FRP in a hybrid system, thus achieving a cost competitive design with several performance gains. Screw lock couplers that cost about 60 USD per unit after machining were used for connecting SMA with steel. This has several advantages over

threaded couplers since it requires neither threading/treatment to the ends of the bars, nor special installation. Such a quick and easy installation can save time and money.

Using proper coupling devices for connecting FRP bars with SMA can reduce slippage substantially, which would eventually help to fully utilize the super-elasticity of SMA. This can bring about significant gains in the construction industry, since corrosion-free ductile FRP RC structures with reduced cracking and permanent deformation can be made. Although, the use of SMA and couplers may increase initial costs, SMA-FRP coupled RC structures will have added advantages over regular structures since there could be no yearly maintenance and replacement costs due to corrosion. Moreover, the structure can be serviceable even after a strong earthquake as it can recover its original position after large deformation, thus requiring a minimum amount of repairing. Considering the present value of the overall lifecycle cost of an RC structure, using FRP bars alone may save approximately 15% to 20% of such a cost [Kostuk et al. 2008]. Use of SMA will further increase the savings since it has high corrosion resistance and possesses large deformation capability with a potential of recovering large deformation after unloading, thus enhancing structural safety.

The present study explored the performance under reversed cyclic loading of concrete BCJs reinforced with SE SMA at their plastic hinge region and FRP in the other regions. Although there are different approaches in the literature for improving the corrosion resistance of RC structures, they had mixed results. For instance, the use of low permeability concrete with added corrosion inhibitors may be used but concrete needs to be crack free, which cannot be guaranteed. Another option is to use epoxy coated reinforcing steel, yet recent field

investigation showed that this will extend the service life of only 5 percent of the structure [Weyers et al. 1997]. Cathodic protection is another alternative for corrosion mitigation in RC members. However, this requires installation of equipment and power supply along with regular operation and maintenance. Conversely, the main advantage of using SMA-FRP RC is that it is corrosion free and should require no additional care or support. However, devoted research efforts are still required to address many issues and uncertainties before the widespread use of coupled SMA-FRP bars as concrete reinforcement. The limited study presented herein is to prove the concept and stimulate further research work, which will focus on the uncertainties of the seismic response and performance of the proposed SMA-FRP hybrid RC elements, and the potential long term benefits of using the proposed structural types in terms of a reduced probability of failure and the expected life-cycle costs.

9. CONCLUSIONS

The use of SE SMA bars in the plastic hinge region and FRP in other regions of a steel-free BCJ has been examined under reversed cyclic loading. The experimental investigation described in the present paper provides an insight into the potential for developing a new generation of ductile, corrosion-free and hybrid RC structures. Based on the experimental observations and analysis of test results, the following conclusions can be drawn.

- The coupled SE SMA-FRP bar produced a force-displacement hysteresis for JBC-4, similar to that of the steel RC joint JBC-1 with reduced stiffness and comparable residual drift. Although the use of SMA at the plastic hinge region of BCJ was supposed to reduce residual drift significantly due to its super-elasticity, the observed residual deformation is likely due to significant slippage of the FRP bar

inside the couplers. However, specimen JBC-4 could still carry 89% of its load capacity beyond the collapse limit. Such corrosion free SMA-FRP RC structural elements could have a great benefit in highly corrosive environments, where it would require little or no maintenance/repairing.

- In the case of the steel-RC beam-column joint specimen JBC-1, the plastic hinge developed at the face of the column. Conversely, the use of SE SMA in the joint region of JBC-4 successfully relocated the plastic hinge region away from the column face to a distance of approximately one-quarter of the beam-depth.
- Specimen JBC-4 dissipated a comparable amount of energy to that of JBC-1. However, its energy dissipation was governed by significant slippage of FRP and SMA bars and extensive cracking of the concrete beam. On the other hand, larger hysteretic loops of steel in the beam hinge region of JBC-1 resulted in a higher amount of energy dissipation compared to that of SMA's smaller hysteretic loops in JBC-4.
- The beam moment rotation relationship of JBC-4 was found different than that of JBC-1 because of the relatively low modulus of elasticity of SMA, which led to delayed yielding of the Ni-Ti bar compared to that of steel. This also caused higher beam rotation in JBC-4 than that of JBC-1 at equivalent beam-tip displacements.
- The strains in the longitudinal SMA bar of specimen JBC-4 experienced negligible residual strain, while longitudinal steel bars of specimen JBC-1 suffered much larger residual strain.

REFERENCES

ACI 440.1R-06, (2006). Guide for the design and construction of concrete reinforced with FRP bars. ACI Committee 440. Technical Report. San Francisco California.

Aiello, M. A., and Ombres, L., (2002). "Structural performances of concrete beams with hybrid (fiber-reinforced polymer-steel) reinforcements." J. *of Comp.for Const.* 6(2), 133-140.

Alam, M. S., Youssef M. A., and Nehdi, M. (2007a) "Utilizing shape memory alloys to enhance the performance and safety of civil infrastructure: A review." *Canadian J. Civil Eng*. 34(9), 1075–1086.

Alam, M. S., Youssef, M. A., and Nehdi, M. (2007b). "Seismic behaviour of concrete beam-column joints reinforced with superelastic shape memory alloys." *Proc. of the 9th Canadian Conf. on Earthquake Eng.*, paper 1125, 10p.

Alam, M. S., Nehdi, M., and Youssef, M. A. (2007c). "Applications of shape memory alloys in earthquake engineering." *Proc. of the 9th Canadian Conf. on Earthquake Eng.*, paper 1124, 10p.

Alam, M. S., Nehdi, M., and Youssef, M. A. (2008). "Shape memory alloy based smart RC bridge: overview of state of the art." *Smart Structures and Systems, an Int. J.* 4(3), 367-389.

Benmokrane, B., Zhang, B., Chennouf, A., and Masmoudi, R. (2000). "Evaluation of aramid and carbon fibre reinforced polymer composite tendons for prestressed ground anchors." *Canadian J. of Civil Eng.*, 27(5), 1031-1045.

Berg, A. C., Bank, L. C., Oliva, M. G., and Russell, J. S. (2006). "Construction and cost analysis of an FRP reinforced concrete bridge deck." *Constr. and Building Mats.*, 20(8), 2006, 515-526.

Choo, C.C. (2005). "Investigation of rectangular concrete columns reinforced or prestressed with fiber reinforced polymer (FRP) bars or tendons." PhD dissertation, University of Kentucky, Lexington, Ky., 155p.

Cole, B., and Fam, A. (2006). "Flexural load testing of concrete-filled FRP tubes with longitudinal steel and FRP rebar." *J. of Comp. for Constr.*, 10(2), 161-171.

CSA A23.3-04. (2004). "Design of Concrete Structures." *Canadian Standards Association*, Rexdale, Ontario, Canada.

Elnashai, A. S., and Broderick, B. M. (1994). "Seismic resistance of composite beam-columns in multi-storey structures. Part 1: Experimental studies." *J. of Constr. Steel Research*, 30(3), 201-229.

Fukuyama, H., Masuda, Y., Sonobe, Y., and Tanigaki, M. (1995). "Structural performances of concrete frame reinforced with FRP reinforcement." *Proc. of 2nd Int. RILEM Symp. on Non-metallic (FRP) Reinf. for Concrete Struct.*, Ghent, Belgium, 275-286.

Grira, M., and Saatcioglu, M. (1999). "Reinforced concrete columns confined with steel or FRP grids." *Proc. of the 8th Canadian Conf on Eq. Eng.*, Vancouver, Canada, 445–450.

Hall, P. C. (2003). "Laser Welding Nitinol to Stainless Steel." *Proc. of the Int. Conf. on Shape Memory and Superelastic Technologies*, California, 219-228.

Kostuk, K. J., Sparks, G. A., Christensen, P. N., and Tadros, G. (2008). Comparing conventional and innovative bridge deck options: A life cycle engineering and costing approach', available online, www.pultrall.com/Site2008/Docs/**LifeCycle**Cost-Kostuk-Sparks-Tadros-Final-Revised.pdf.

Leung, H. Y., and Balendran, R. V. (2003) "Flexural behaviour of concrete beams internally reinforced with GFRP rods and steel rebars." *Structural Survey*, 21(4), 146-157.

Nehdi, M., and Said, A. (2005). "Performance of RC frames with hybrid reinforcement under reversed cyclic loading." *Materials and Structures*, 38(6), 627-637.

Paulay, T., and Priestley, M. N. J. (1992). "Seismic design of reinforced concrete and masonry buildings." John Wiley & Sons Inc. New York.

Said, A., and Nehdi, M. (2004). Use of FRP for RC frame in seismic zones: Part II. Performance of steel free GFRP-reinforced beam-column joints." *Applied Composite Materials*, 11, 227-245.

Saiidi M. S., and Wang H. (2006). "Exploratory study of seismic response of concrete columns with shape memory alloys reinforcement." *ACI Struct. J.* 103(3), 435–442.

Saikia, B., Thomas, J., Ramaswamy, A., and Rao, K. S. N. (2005). "Performance of hybrid rebars as longitudinal reinforcement in normal strength concrete." *Mat. and Struct.* 38(10), 857-864.

Salib, S. R. and Abdel-Sayed, G. (2004). "Prediction of crack width for fiber-reinforced polymer-reinforced concrete beams." *ACI Struct. J.*, 101(4), 532-536.

Sharbatdar, M. K., and Saatcioglu, M. (2009). "Seismic design of FRP reinforced concrete structures." *Asian J. of Applied Sc.*, 2(3): 211-222.

Toutanji, H. A., and Saafi, M. (2000). "Flexural behavior of concrete beams reinforced with glass fiber-reinforced polymer (GFRP) bars." *ACI Struct. J.*, 97(5), 712-719.

Udhayakumar, V., Bharatkumar, B. H., Balasubramanian, K., Krishnamoorthy, T. S., and Lakshmanan, N. (2007). "Experimental investigations on flexural behaviour of RC slabs reinforced with GFRP rebars." J. of the Inst. of Engrs. (India): Civil Eng. Div., 88(11), 23-27.

Wang, H. (2004). “A study of RC columns with shape memory alloy and engineered cementitious composites.” *M.Sc. Thesis, Dept. of Civil Eng., Uni. of Nevada, Reno.*

Weyers, R. E., Pyc, W., Zemajtis, J., Liu, Y., Mokarem, D., Sprinkel, M. M. (1997). “Field investigation of corrosion-protection performance of bridge decks constructed with epoxy-coated reinforcing steel in Virginia.” Transportation Research Record: J of the Transportation Research Board, 1597, 82-90.

Wilson, J. C. and Wesolowsky, M. J. (2005). “Shape memory alloys for seismic response modification: a state-of-the-art review.” *Earthquake Spectra*, 21(2), 569-601.

Won, J.-P. and Park, C.-G. (2006). “Effect of environmental exposure on the mechanical and bonding properties of hybrid FRP reinforcing bars for concrete structures.” J. of Comp. Mat., 40(12), 1063-1076.

Youssef, M. A., Alam, M. S. and Nehdi, M. (2008). “Experimental investigation on the seismic behaviour of beam–column joints reinforced with superelastic shape memory alloys', *J. Earthquake Eng.* 12(7), 1205-1222.

Table 1

Comparative results of the specimens JBC-1 and JBC-4 Performance Parameter	JBC-1	JBC-4
First flexural Crack Load (kN)	11.7	13.5
Drift at first flexural crack (%)	0.22	0.22
Yield load (kN)	51.3	34.1
Drift at yield load (%)	1.30	1.97
Load at 3% drift (kN)	60.0	57.5
Load at 4% drift (kN)	61.0	52.0
Residual drift after 4% drift (%)	1.8	2.0
Energy dissipation after 3% storey drift (kN)	3.4	3.1
Energy dissipation after 4% storey drift (kN)	6.29	6.76
Beam rotation at 4% storey drift (rad)	0.006	0.0095
Residual beam rotation after 4% storey drift (rad)	0.0042	0.012

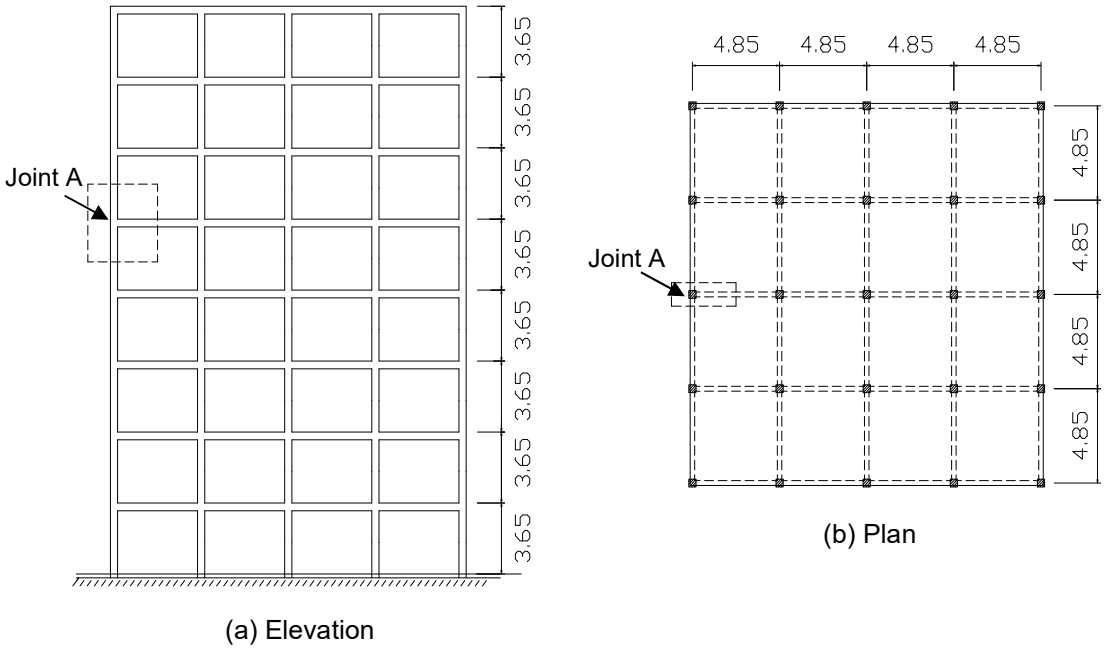

(a) Elevation

(b) Plan

Fig. 1. Eight-storey frame building located in the western part of Canada (dimensions in meters).

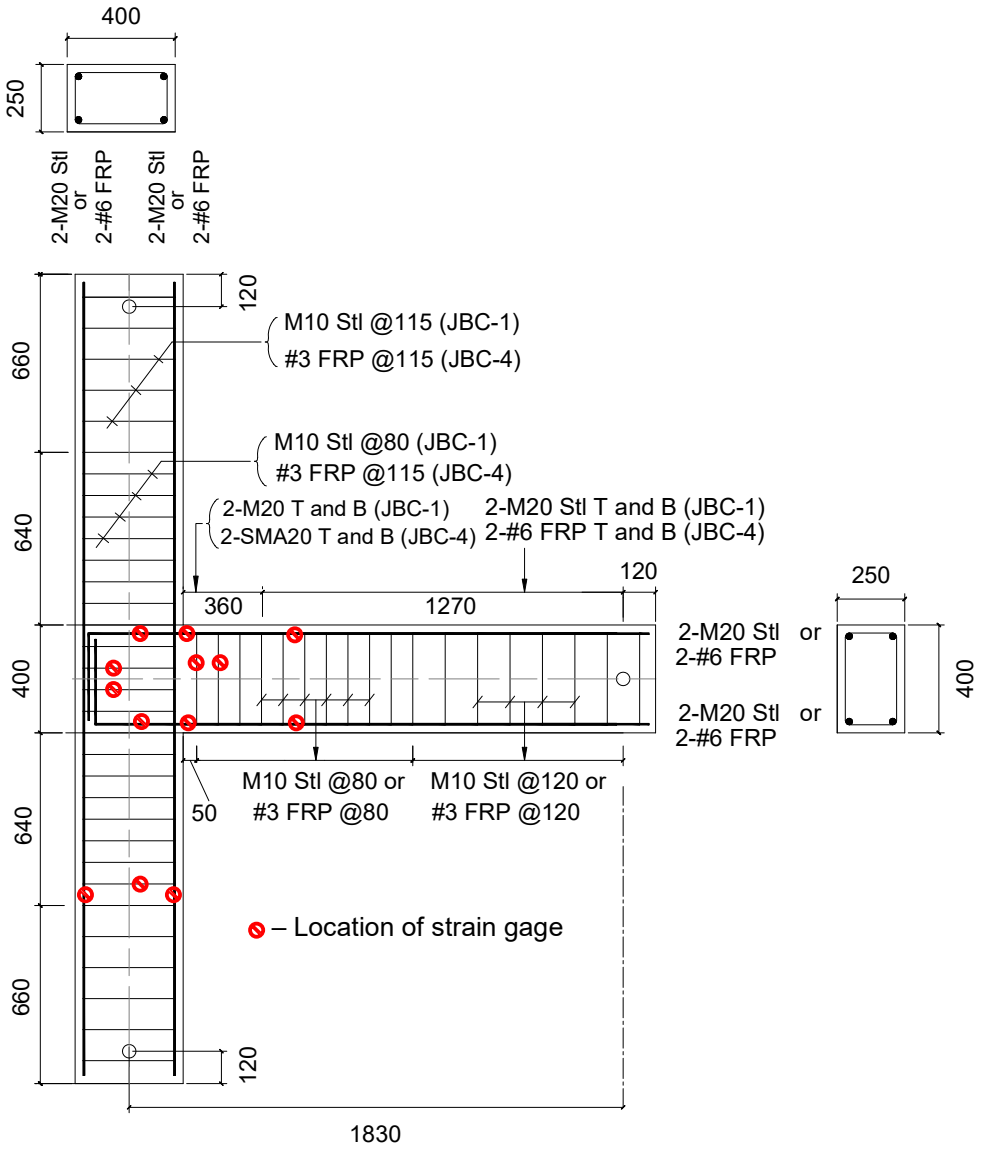

Fig. 2. Reinforcement details of specimen JBC1 and JBC4 (dimensions in mm).

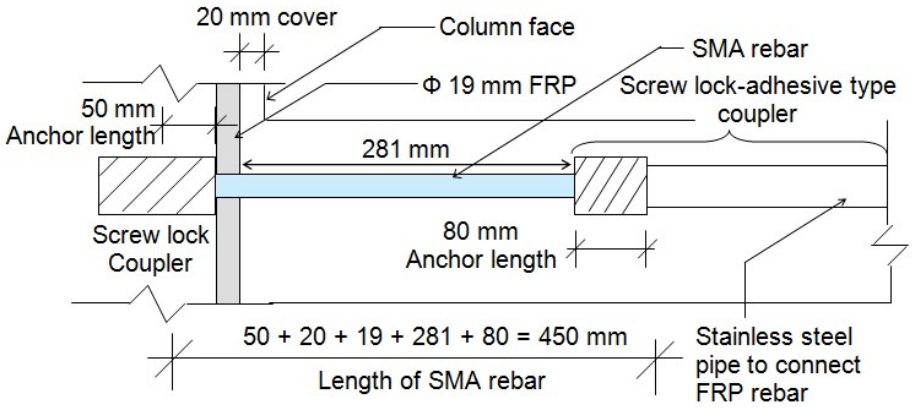

Fig. 3. Length of SMA rebar

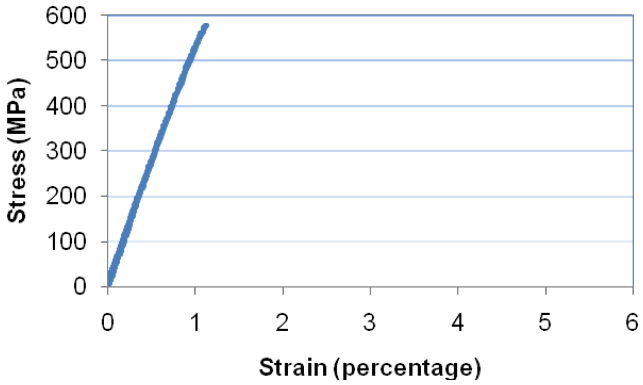

(a)

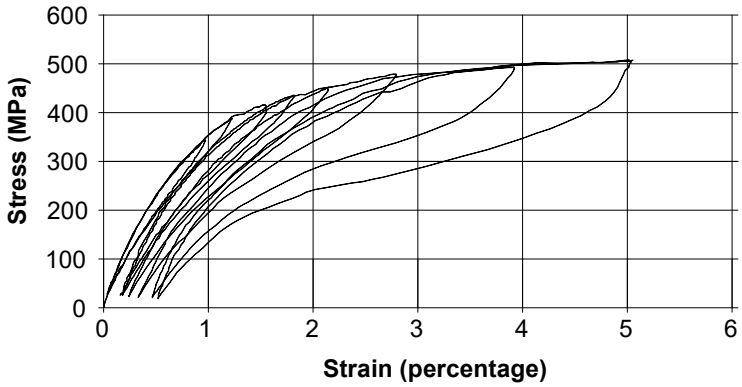

(b)

Fig. 4. (a) Cyclic tensile strength of SE SMA bar within the screw-lock coupler, and (b) cyclic tensile strength of GFRP bar within the adhesive type coupler.

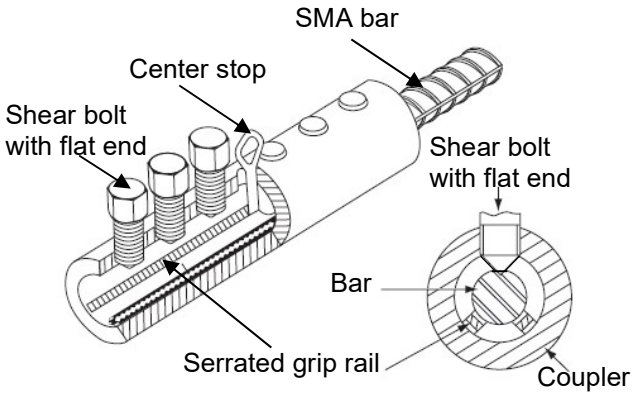

Fig. 5. Regular single barrel screw-lock coupler.

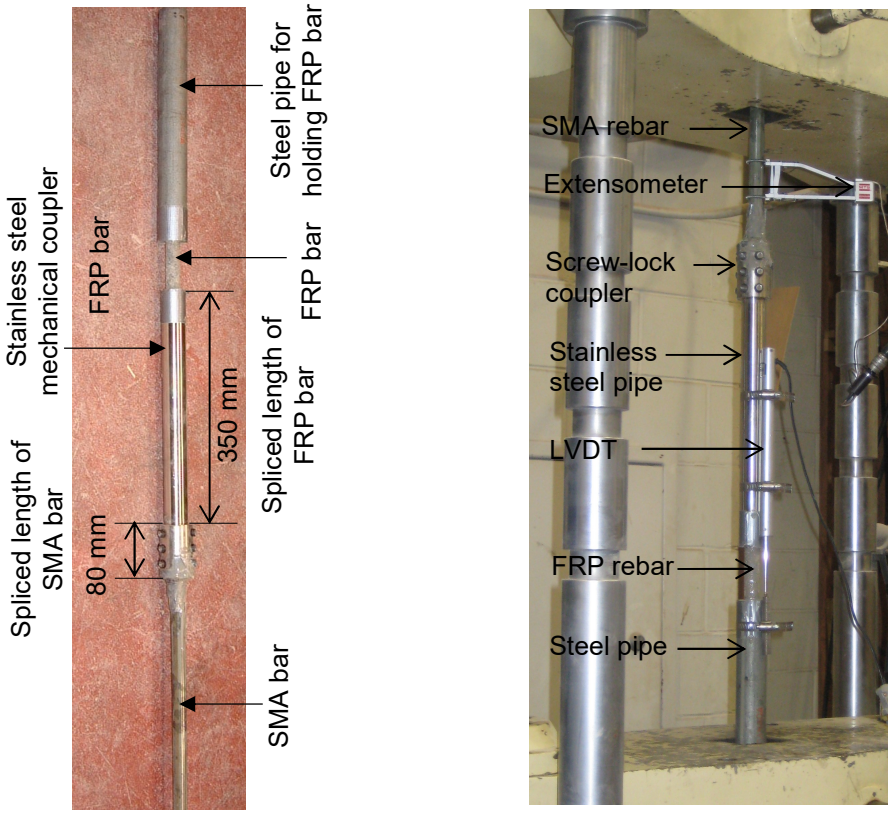

Fig. 6. (a) Test specimen: screw lock-adhesive type coupler connecting FRP with SMA bar, (b) testing of the splice connection of FRP and SMA using the screw lock-adhesive type coupler.

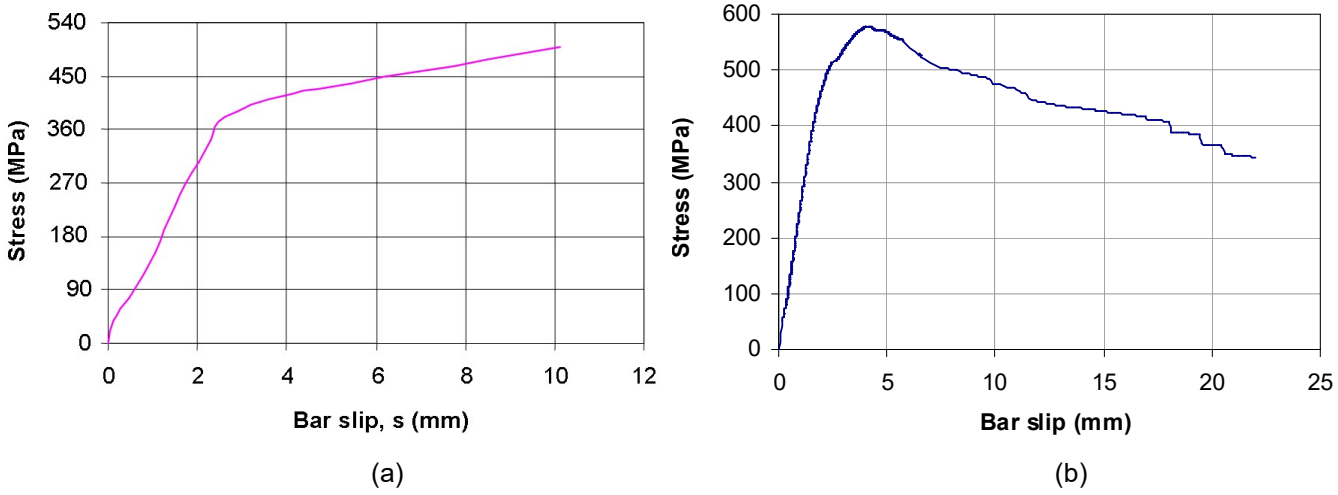

Fig.7. Stress versus slippage of (a) SMA bar, and (b) FRP bar inside the screw lock-adhesive type coupler.

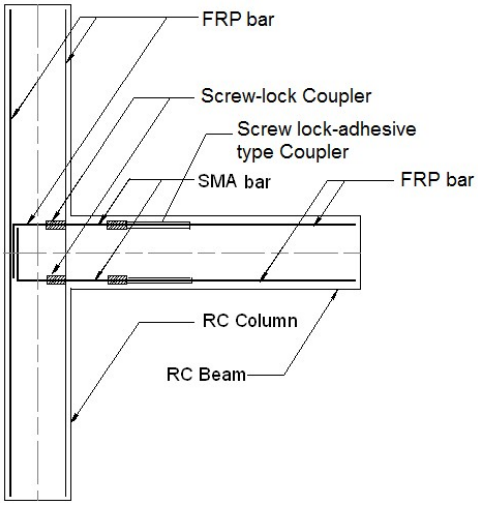

Fig. 8. Splice details of specimen JBC4.

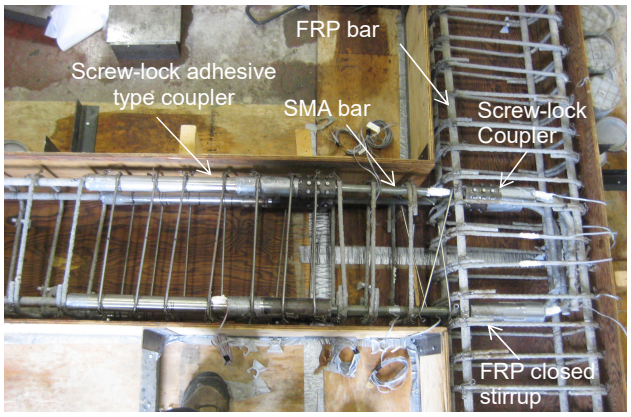

Fig. 9. Reinforcement cage of JBC4 showing the bar and coupler arrangements inside the formwork.

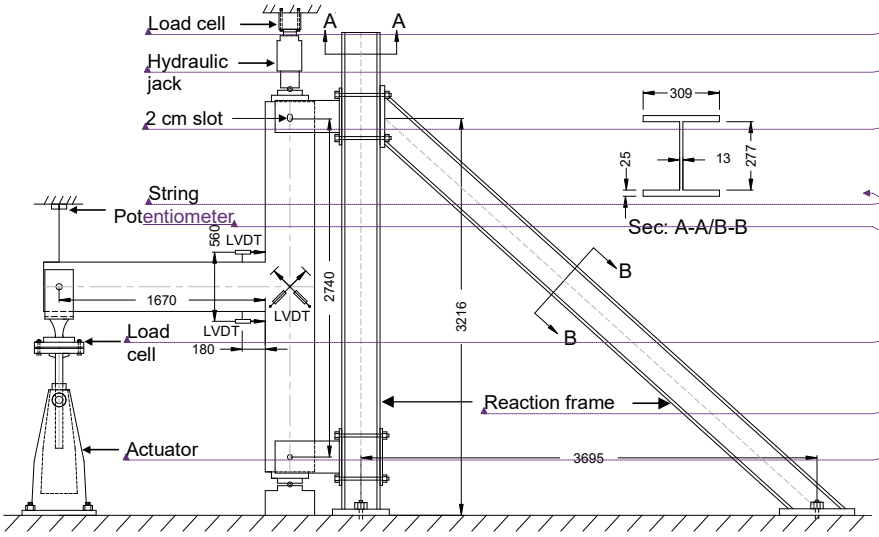

Fig. 10. Test setup (all dimensions in mm).

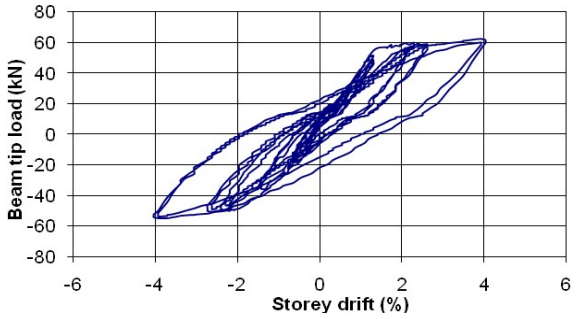

Fig. 11. Beam tip load-storey drift relationship of specimen JBC1.

Formatted: Font: 9.5 pt, Complex Script Font: 9.5 pt

Formatted: Font: 9.5 pt, Complex Script Font: 9.5 pt

Formatted: Font: 9.5 pt, Complex Script Font: 9.5 pt

Formatted: Font: 9.5 pt, Complex Script Font: 9.5 pt

Formatted: Centered

Formatted: Font: 9.5 pt, Complex Script Font: 9.5 pt

Formatted: Font: 9.5 pt, Complex Script Font: 9.5 pt

Formatted: Font: 9.5 pt, Complex Script Font: 9.5 pt

Formatted: Font: 9.5 pt, Complex Script Font: 9.5 pt

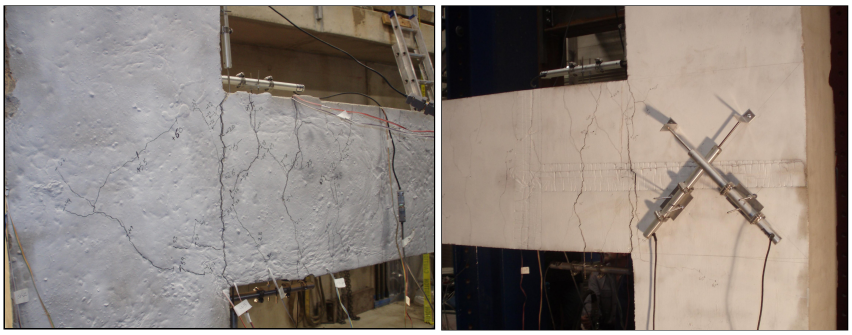

(a) (b)

Fig. 12. Crack pattern of specimen JBC1 after being subjected to cycles up to 4% drift (a) front face, and (b) rear face.

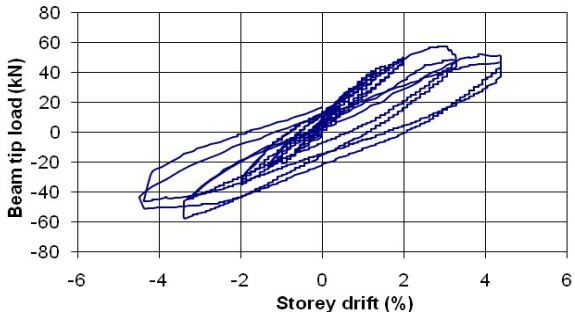

Fig. 13. Beam tip load-storey drift relationship of specimen JBC-4.

(a) (b)

Fig. 14. Crack pattern of specimen JBC-4 after being subjected to cycles up to 4.4% drift (a) front face, and (b) rear face.

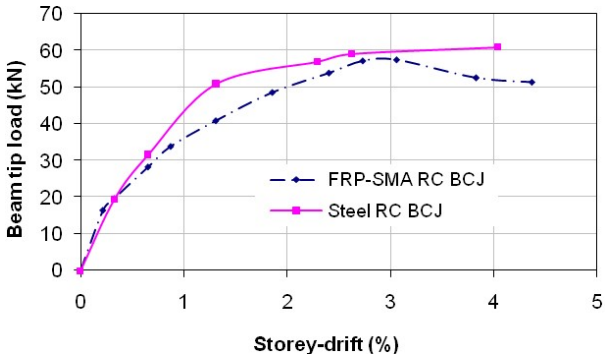

Fig. 15. Beam tip-load versus storey drift envelope of the tested specimens JBC1 and JBC4.

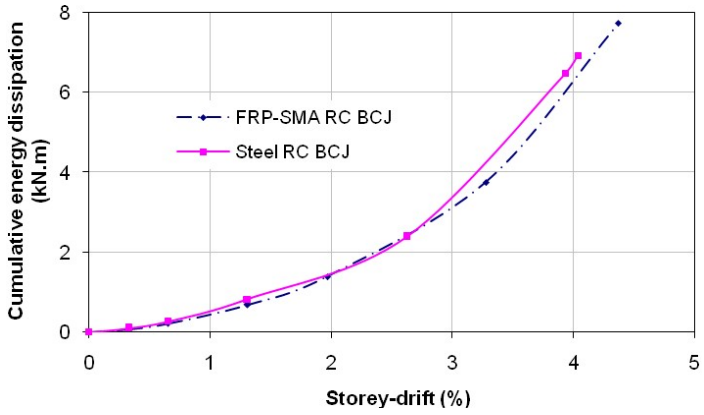

Fig. 16. Cumulative energy dissipation-storey drifts relationship of specimens JBC1 and JBC4.

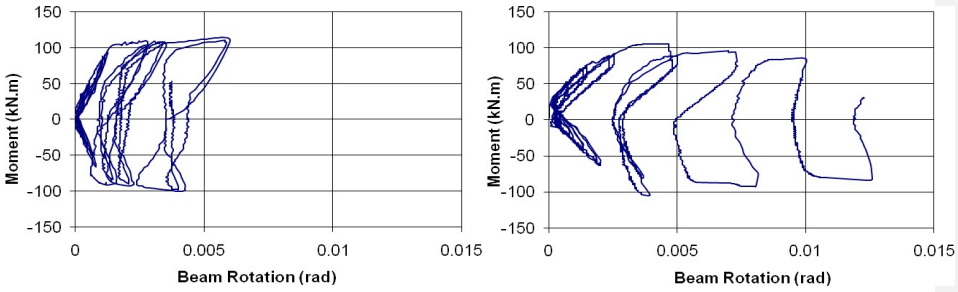

(a) (b)

Fig. 17. Beam moment-rotation plot at 180mm from column face of specimen JBC1 and JBC4.

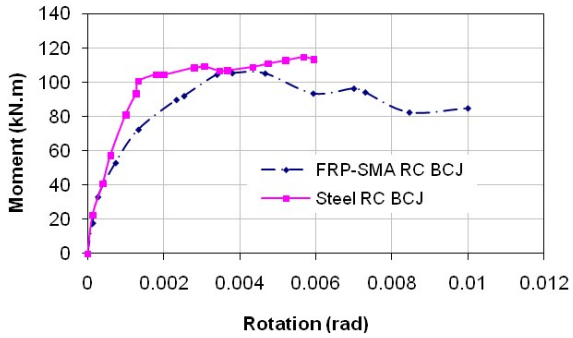

Fig. 18. Beam moment versus rotation envelope of the tested specimens JBC1 and JBC2.

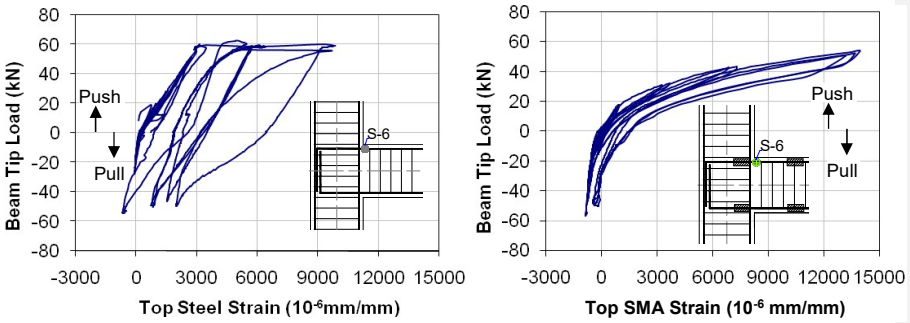

(a) (b)

Fig. 19. Beam tip load versus top reinforcement strain of (a) steel bar of JBC1, and (b) SMA bar of JBC4.

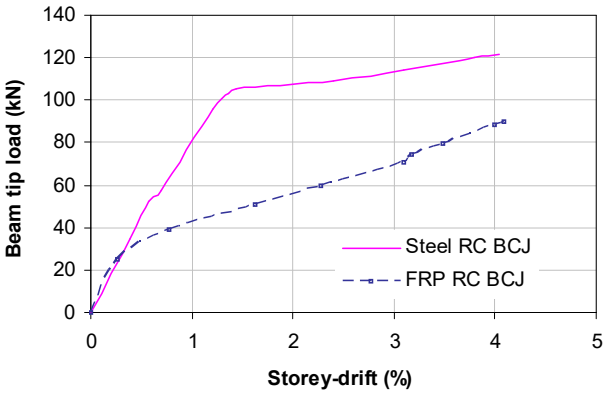

Fig. 20. Beam tip load versus storey-drift envelope of J1 and J4 [27].

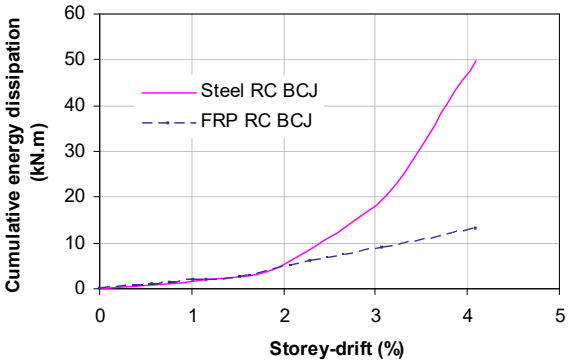

Fig. 21. Cumulative energy dissipation capacities of J1 and J4 [27].